Materials Science & Engineering A 596 (2014) 41–44

Contents lists available at ScienceDirect

Materials Science & Engineering A

journal homepage: www.elsevier.com/locate/msea

Rapid communication

Observation and Schmid factor analysis of multiple twins in a warm-rolled Mg–3Al–1Zn alloy

Renlong Xin [a,*], Maoyin Wang [a], Xiaoxu Huang [a,b], Changfa Guo [a], Qing Liu [a]

[a] College of Materials Science and Engineering, Chongqing University, Chongqing 400045, China
[b] Danish–Chinese Center for Nanometals, Materials Research Department, Risø National Laboratory for Sustainable Energy, Technical University of Denmark, DK-4000 Roskilde, Denmark

ARTICLE INFO

Article history:
Received 12 August 2013
Received in revised form
4 November 2013
Accepted 9 December 2013
Available online 16 December 2013

Keywords:
Twinning
Magnesium alloy
Schmid factor
Texture

ABSTRACT

This study aims to understand the features of twinning that occurred during warm-rolling of Mg–3Al–1Zn alloys. The rolling was performed at 150 °C with the *c*-axis of most grains nearly parallel to the transverse direction. Electron backscatter diffraction analysis was conducted to examine microstructural evolution of the rolled sample. Multiple twins including {10−12} extension twin, {10−11} contraction twin, {10−11}–{10−12} and {10−12}–{10−11} double twins and {10−12}–{10−11}–{10−12} tertiary twins were observed in the rolled sample. These twins were present even in the same grain orientation. Based on the applied rolling deformation, an effective Schmid factor was calculated to understand the activation of twinning. Calculated Schmid factor maps were obtained as a function of (0001) pole. The activation of {10−12}–{10−11} double twin was explained by the statistical analysis of Schmid factors for primary {10−12} twin and secondary {10−11} twin.

1. Introduction

For hexagonal close packed Mg alloys, the number of independent slip systems is limited especially at low temperature, which results in poor workability and hinders their wider applications. Twinning is an important deformation mechanism for Mg alloys, which significantly impacts the micro- and macroscopic properties of wrought Mg products [1–4]. For example, Barnett has reviewed the twinning and the ductility of Mg alloys and pointed out that twinning can significantly affect the uniform elongation of Mg alloys and the effect is dependent on the mode of twinning [2,3]. During twinning, grains can be subdivided and texture can be tailored, which has recently been utilized to improve the yield asymmetry of rolled Mg plates [4]. Because of the above mentioned importance, a deeper understanding of twining features is essential for the development of new Mg alloys and novel processing methods.

The most commonly reported twinning modes include {10−12}⟨−1011⟩ extension twin, {10−11}⟨10−1−2⟩ contraction twin, {10−11}–{10−12} and {10−13}–{10−12} double twins [5–8]. These types of twins have been extensively observed in previous studies on deformed Mg alloys. The features of the twins and their correlation with deformation conditions have been relatively well understood. For example, Jiang et al. reported that the initial extrusion texture plays an important role in the formation of different types of twins, and that the twinning behavior also depends on the strain path [9]. Park et al. revealed that the {10−12} extension twinning characteristics were significantly dependent on the activation mode (i.e., tension parallel or compression perpendicular to the *c*-axis of grains) [10]. Ma et al. studied the twinning mechanism in a {10−10}-fiber textured Mg alloy and reported a two-shear mode mechanism for the nucleation of {10−11}–{10−12} and {10−13}–{10−12} double twins [11]. However, most of the previous studies dealt with the formation of twins in uniaxial deformations; only a few studies examined the detailed features of twinning in rolling (plane strain compression) or bending deformations [12–14], despite its importance in understanding the deformation mechanism of Mg alloys during hot-working and forming processes.

Recently primary, secondary and tertiary twins have been observed in Mg alloys deformed in plane strain compression in a channel die [12], indicating that twinning may be more complex in rolling conditions than uniaxial deformations. The previous study has analyzed in depth the variant selections of the complex twins in plane strain compression [12]. However, why multiple twins are favored in rolling conditions is still not very clear. So the present study aims to examine the features of twinning during warm-rolling of Mg alloys. The studied alloy has a *c*-axis//transverse direction texture (named as TD texture), which is different from that in [12] (with *c*-axis parallel to the elongated direction). Multiple twins were observed in the rolled Mg samples, and

* Correspondence to: Sha Zheng Jie 174#, Sha Ping Ba District, Chongqing, China. Tel.: +86 23 65102179; fax: +86 23 65106407.
E-mail address: rlxin@cqu.edu.cn (R. Xin).

0921-5093/$ - see front matter © 2013 Elsevier B.V. All rights reserved.
http://dx.doi.org/10.1016/j.msea.2013.12.030

effective Schmid factors (SFs) were calculated based on the applied rolling deformation to explain the activation of the complex twins.

2. Experimental

The TD textured plate samples were prepared from a 70 mm thick Mg–3Al–1Zn sheet which originally presents a typical basal texture. The samples were cut in such a way as to allow the *c*-axis of grains to be approximately parallel to the TD for rolling as illustrated in Fig. 1a (the inset). The samples were rolled by one pass with a rolling speed of ~1.2 m/s at ~150 °C. The microstructure of the rolled sample (with ~11% reduction) was examined from the center part of the rolled sample by electron backscatter diffraction (EBSD).

3. Results and discussion

The typical EBSD microstructure of rolled samples is shown in Fig. 1a, in which and also in Figs. 1b, 2a and 3a, the high angle grain boundary (⟩15°) is highlighted by a black line. The {10−12} twin boundary (86±5° ⟨1−210⟩), {10−11} twin boundary (56±5° ⟨1−210⟩) and {10−11}–{10−12} double twin boundary (38±5° ⟨1−210⟩) are highlighted by green, yellow and cyan lines, respectively. As seen from Fig. 1a, there are a number of {10−12} twin boundaries, indicating that {10−12} twin is favorable during rolling of the TD textured Mg plates. In addition, a few {10−11} twin and {10−11}–{10−12} double twin boundaries are observed. Generally {10−11} twin bands are very thin (narrow-banded) whereas {10−12} twin bands are rather broad (lenticular-like). In some cases, more than one type of twin occurs under the same grain orientation. For example, in Fig. 1b both {10−12} twin (indicated by 1ET) and {10−11} twin (indicated by 1CT) are observed in the same grain. The orientation relationships among the twins and parent grain are illustrated in (0001) pole figures, as shown in Fig. 1c. The SFs of active variants are indicated in the pole figures. The definition of the SFs in rolling deformations will be detailed later. Hexagonal cells are presented as the inset in Fig. 1b, which indicates that the disorientation axis between 1CT and the parent grain is different from that between 1ET and the parent grain.

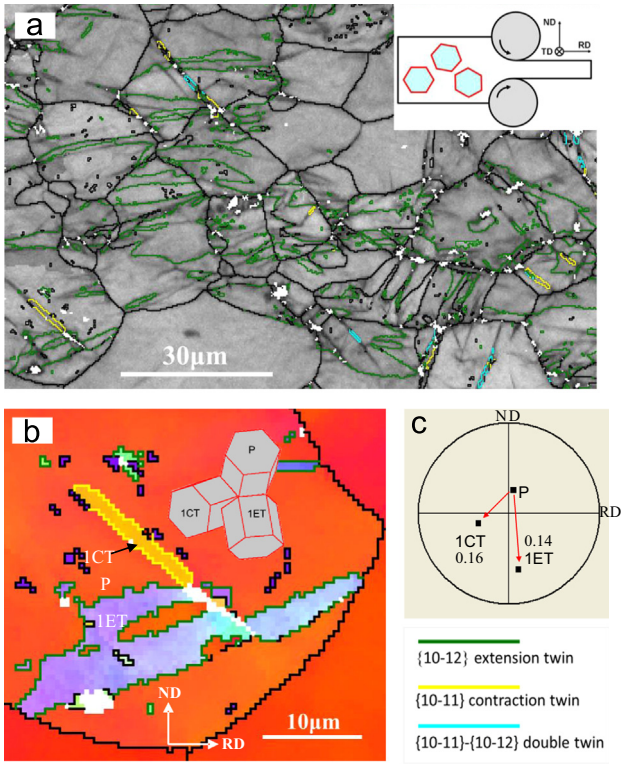

Fig. 1. (a) EBSD map of TD textured AZ31 rolled ~11% reduction at 150 °C. (b) EBSD map showing the {10−12} twin (indicated by 1ET) and {10−11} twin (indicated by 1CT) observed in the same grain. Negative SF values are highlighted in gray. (c) (0001) pole figure showing the crystallographic orientations of the parent and twins in (b). The inset in (a) illustrates the orientation of *c*-axis with respect to the applied rolling deformation. The SFs of active variants are presented in the pole figure. (For interpretation of the references to color in this figure, the reader is referred to the web version of this article.)

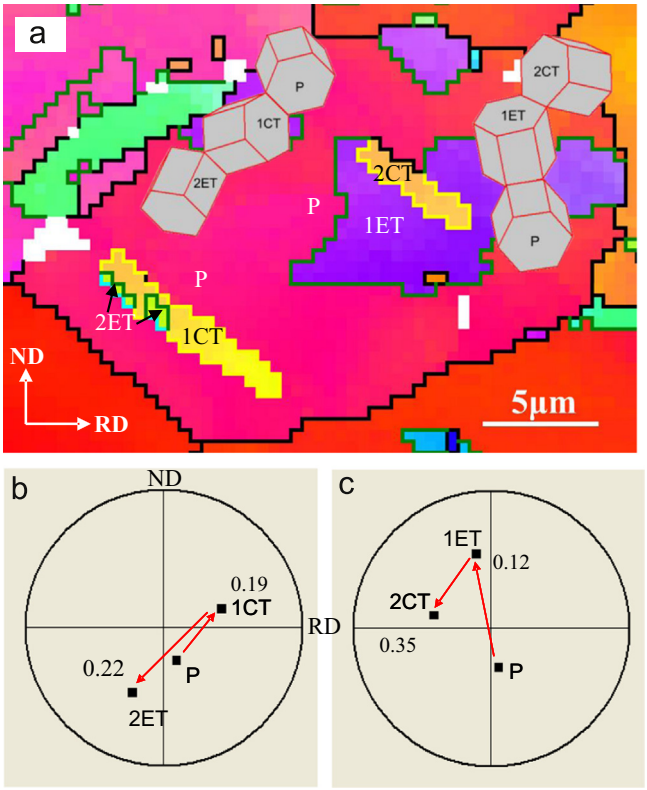

Fig. 2. EBSD map showing the formation of two types of double twins: {10−11}–{10−12} and {10−12}–{10−11} (indicated by 1CT–2ET and 1ET–2CT, respectively). (b), (c) (0001) pole figures showing the crystallographic orientations of the two types of double twins. The SFs of active variants are presented in the pole figure. (For interpretation of the references to color in this figure, the reader is referred to the web version of this article.)

In the rolled Mg alloys both {10−11}–{10−12} and {10−12}–{10−11} double twins were observed. Sometimes the two types of double twins can occur in the same grain. As confirmed by EBSD analyses in Fig. 2a, the narrow yellow band in the left-bottom of the grain (indicated by 1CT) is {10−11} twin. The green areas within 1CT are {10−12} twin (indicated by 2ET). Apparently 1CT and 2ET consist of the commonly reported {10−11}–{10−12} double twin, namely, CT–ET double twin. Moreover, a few purple areas are present in the same grain, which are primary {10−12} twins. Inside one of the {10−12} twins (indicated by 1ET), there is a narrow yellow band (indicated by 2CT), which is {10−11} twin formed inside {10−12} twin. Apparently 1ET and 2CT consist of a {10−12}–{10−11} double twin, namely, ET–CT double twin. Note that the sequence of CT and ET is opposite in these two types of double twins. The orientation relationships between the twins and the parent grain are illustrated in (0001) pole figures (Fig. 2b and c) and by hexagonal cells (insets in Fig. 2a). It indicates that the disorientation axis between 1CT and the parent grain is parallel to that between 2ET and 1CT in the CT–ET double twin. The theoretical disorientation between 2ET and the parent grain is

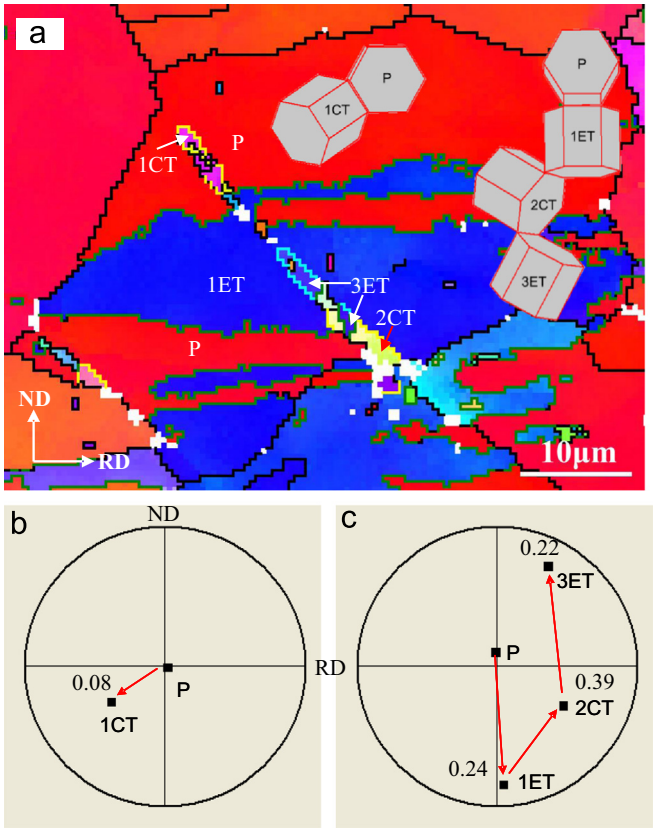

Fig. 3. (a) EBSD map showing a {10−12}–{10−11}–{10−12} tertiary twin (indicated by 1ET–2CT–3ET). A primary {10−11} twin (indicated by 1CT) is also seen on the left-top. (b), (c) (0001) pole figures showing the crystallographic orientations of the primary and tertiary twins. The SFs of active variants are presented in the pole figure. (For interpretation of the references to color in this figure, the reader is referred to the web version of this article.)

38°/⟨1–210⟩, which is the most likely a selected variant of {10−11}–{10−12} double twins according to [13,15,16]. For the ET–CT double twins the disorientation axis between 1ET and the parent grain is different from that between 1ET and 2CT. The theoretical disorientation between 2CT and the parent grain is determined to be 70°/⟨−7 14 −7 3⟩. This is the same as one of the 36 possible misorientation relationships for {10−11}–{10−12} double twins as reported in [15].

{10−12}–{10−11}–{10−12} tertiary twin was also observed in the rolled sample. Fig. 3 presents such an example, in which the red areas in the grain have orientations close to the initial TD texture and hence are considered as the residual matrix. The blue area (indicated by 1ET) is a primary {10−12} twin. Inside 1ET, there is a narrow band outlined with yellow and cyan lines. The yellow part (indicated by 2CT) of the band is {10−11} twin formed inside 1ET and is considered as a secondary twin of the parent. The blue part (indicated by 3ET) is a {10−12} twin formed inside 2CT and is therefore considered as a tertiary twin of the parent. So it is a {10−12}–{10−11}–{10−12} tertiary twin, similar to that reported recently by Mu et al. [12]. It should be mentioned that the deformation geometry is different with respect to the *c*-axis of grains in the two studies. In Mu et al.'s study, the *c*-axis of grains is approximately parallel to longitudinal direction (being elongated in the plane strain compression test) while in the present paper it is parallel to TD. In both cases, complicated stress state might exist in the deformed samples. In addition, there is a pink narrow band (indicated by 1CT) within the same grain of Fig. 3a (on left-top), which is identified as {10−11} twin. The orientations of the twins and the parent grain are illustrated in {0001} pole figures (Fig. 3b and c) and by hexagonal cells (the insets in Fig. 3a). The disorientation axis between 1ET and 2CT is parallel to that between 2CT and 3ET, but different from that between 1ET and the parent grain. Interestingly, the theoretical disorientation between 2CT and the parent grain is the same as that of the {10−12}–{10−11} double twin shown in Fig. 2c. But it is not clear whether this is a preferred variant of {10−12}–{10−11} double twin because of a limited volume of data set.

Twinning activity has been commonly evaluated by a global SF defined as $m=\cos\varphi\times\cos\lambda$, where φ (λ) is the angle between the twinning plane normal (twinning shear direction) and the external stress direction. This is mainly applicable for uniaxial deformations [17]. For rolling deformations, as recently reported in [13] twinning behavior can be reasonably predicted by an effective SF defined as $m=0.5\times(\cos\varphi_{RD}\times\cos\lambda_{RD}-\cos\varphi_{ND}\times\cos\lambda_{ND})$, where $\varphi_{(RD,\ ND)}$ is the angle between twinning plane normal and the rolling or normal direction. $\lambda_{(RD,\ ND)}$ is the angle between twinning shear direction and the rolling or normal direction. Being consistent with [13], the SF is defined as positive (negative) when the twin strain has a component corresponding to extension along RD (contraction along ND). As explained in [13], the minus sign in the equation takes care of the fact that a favored twinning mode will give extension along RD but contraction along ND and hence a large effective SF. The value of 0.5 is just for normalization purposes. This effective SF definition is used throughout the paper.

As indicated in (0001) pole figures of Figs. 1–3, all the twins have positive SFs, meaning that the normal strains generated by twins are compatible with the applied rolling deformation. In some cases the selected variant does not have the highest SF, which is probably affected by local stress or strain conditions. The variant selection of twins in Mg alloys has been well studied earlier and is not a subject here [12]. To further understand why {10−12} twin and {10−11} twin can occur in the same grain for this applied rolling deformation, SFs are calculated as a function of crystal orientations and presented in (0001) pole figures. As is known, each point in the pole figure represents a set of orientations (with $\varphi1$ and φ fixed; $\varphi2$ varying from 0° to 60°). All possible orientations were considered in this calculation. But for simplicity only the maximum SFs are presented in Fig. 4a and b. The calculation results indicate that the SFs for {10−12} twin and {10−11} twin are largely affected by *c*-axis orientations. But they are less affected by $\varphi2$, i.e., the change of orientations around the *c*-axis. More importantly, Fig. 4a and b shows that for grains oriented around the TD, both {10−12} twin and {10−11} twin are favorable for this applied rolling deformation. This is consistent with the results presented in Figs. 1c, 2b, c and 3c, in which all the parent grains have orientations close to TD. According to [13], the larger SF indicates the better compatibility between the normal strains due to twinning and the applied rolling deformation. This might be one reason for the observation of complex twinning in the rolled TD textured sample. The superior activity of {10−12} twin over {10−11} twin is due to the low CRSS of the former. Moreover, there is actually small extension strain in TD during practical rolling processes, which is also favorable for the activation of the {10−12} twin.

To understand why {10−12}–{10−11} double twin was likely activated in the rolled sample the following SF calculation is performed. First, 396 initial grains were extracted from EBSD data of the initial sample. The mean orientation of each grain was determined by a quaternion vector method [18] and is represented by red squares in Fig. 4c. Second, the orientations of primary {10−12} twins (1ET) were obtained by rotating the orientations of the parent grains by 180° around the mostly stressed twinning plane normal. The obtained orientations of 1ET are represented by blue squares in Fig. 4c. Third, the SFs for 1ET and secondary {10−11} twin (2CT) were calculated based on the orientations of

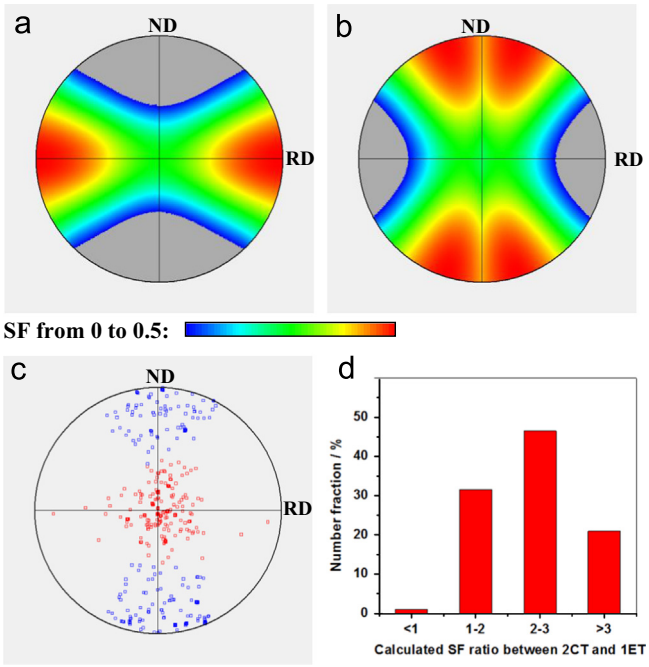

Fig. 4. Calculated SFs for twins as a function of (0001) pole for this applied rolling deformation: (a) {10 – 12} twin; (b) {10 – 11} twin. (c) 396 representative grains and the {10 – 12} twinned orientations under rolling in the (0001) pole figure. Red squares represent the parent grains and blue squares represent the {10 – 12} twins. (d) Number fraction vs. the ratio of SFs for primary {10 – 12} twin over that for secondary {10 – 11} twin. The SFs are calculated based on the orientations presented in (c). (For interpretation of the references to color in this figure legend, the reader is referred to the web version of this article.)

the parent grains and 1ET. Then the activation easiness of 1ET and 2CT can be evaluated by comparing their SFs for each single grain. Here, only the highest SF variant is used for comparison. This is reasonable because the highest SF variant is the most likely selected for {10 – 12} and {10 – 11} twinning (though abnormal twin has been observed in some cases [16]). Fig. 4d presents the comparison results of SFs for 1ET and 2CT in the 396 individual grains. It shows that ~67% grains have the SF ratio of 2CT/1ET larger than two, and ~21% grains have the ratio over three. Moreover, in all the 396 analyzed grains, the SF for 2CT is larger than 0.3. The above analyses indicate that 2CT is more favorable than 1ET in terms of SF in this applied rolling deformation. This is considered as one major reason for the activation of {10 – 12}–{10 – 11} double twins during rolling. The high strain rate of rolling may also favor the nucleation of 2CT instead of the growth of 1ET during the rolling process.

The above mentioned multiple twins were observed in the TD textured AZ31 Mg alloy under warm-rolling conditions. It is interesting to compare them with the twins obtained from the cold-rolled and hot-rolled conditions. Li et al. have studied the twinning features in ME20 Mg alloy subjected to hot-rolling at 400 °C and also observed the presence of {10 – 12} twin and {10 – 11} twin in the same grain [19]. In a previous study on AZ31 Mg alloy by hot-rolling at 300 °C, both {10 – 12} twin and {10 – 11} twin have been observed in rolled samples [20]. These experimental reports are consistent with the SF calculations shown in Fig. 4a and b that for this applied rolling deformation (i.e., the *c*-axis//TD), both {10 – 12} twin and {10 – 11} twin are allowed. However, the {10 – 12}–{10 – 11} double twin and {10 – 12}–{10 – 11}–{10 – 12} tertiary twin have not been reported from the hot-rolling conditions. By applying cold-rolling along the TD, profuse {10 – 12} twin can be activated, but {10 – 11} twin and multiple twins can seldom be observed [4]. It is considered that rolling temperature can affect the activation of different twinning and dislocation slip modes and hence the twinning features. In the above discussed work, the *c*-axis of most grains was kept nearly parallel to the TD of rolling. However, previous studies indicated that the initial grain orientation relative to rolling (i.e., initial texture) can largely affect the mode and characteristics of twinning [19,21]. Therefore, during a rolling process, the sample texture and rolling temperature should be considered to tailor twinning behaviors and hence the microstructural evolution and mechanical properties of rolled sheets.

4. Conclusion

In summary, {10 – 12} twin, {10 – 11} twin, {10 – 12}–{10 – 11} and {10 – 11}–{10 – 12} double twins and {10 – 12}–{10 – 11}–{10 – 12} tertiary twin were observed in a TD textured Mg–3Al–1Zn subjected to warm rolling at 150 °C. These different types of twins can be activated even in the same grain orientations. Analyses of effective SFs confirm that the applied rolling deformation favors the activation of these complex twins.

Acknowledgments

This project was financially supported by the Natural Science Foundation of China (Grant no. 50890172) and the National Basic Research Program of China ("973" Project) (Grant no. 2013CB632200).

References

[1] J.W. Christian, S. Mahajan, Prog. Mater. Sci. 39 (1995) 1–157.
[2] M.R. Barnett, Mater. Sci. Eng. A 464 (2007) 1–7.
[3] M.R. Barnett, Mater. Sci. Eng. A 464 (2007) 8–16.
[4] B. Song, R.L. Xin, G. Chen, X.Y. Zhang, Q. Liu, Scr. Mater. 66 (2012) 1061–1064.
[5] R.E. Reed-Hill, Trans. Metall. Soc. AIME 218 (1960) 554–558.
[6] E.W. Kelley, W.F. Hosford Jr., Trans. Metall. Soc. AIME 242 (1968) 5–13.
[7] B.C. Wonsiewicz, W.A. Backofen, Trans. Metall. Soc. AIME 239 (1967) 1422–1431.
[8] S.L. Couling, J.F. Pashak, L. Sturkey, Trans. ASM, 51, 94–107.
[9] L. Jiang, J.J. Jonas, Scr. Mater. 58 (2008) 803–806.
[10] S.H. Park, S.G. Hong, C.S. Lee, Scr. Mater. 62 (2010) 202–205.
[11] Q. Ma, H. El Kadiri, A.L. Oppedal, J.C. Baird, M.F. Horstemeyer, M. Cherkaoui, Scr. Mater. 64 (2011) 813–816.
[12] S.J. Mu, J.J. Jonas, G. Gottstein, Acta Mater. 60 (2012) 2043–2053.
[13] J.R. Luo, A. Godfrey, W. Liu, Q. Liu, Acta Mater. 60 (2012) 1986–1998.
[14] J.C. Baird, B. Li, S.Y. Parast, S.J. Horstemeyer, L.G. Hector Jr., P.T. Wang, M. F. Horstemeyer, Scr. Mater. 67 (2012) 471–474.
[15] É. Martin, L. Capolungo, L. Jiang, J.J. Jonas, Acta Mater. 58 (2010) 3970–3983.
[16] J.J. Jonas, S. Mu, T. Al-Samman, G. Gottstein, L. Jiang, E. Martin, Acta Mater. 59 (2011) 2046–2056.
[17] S. Godet, L. Jiang, A.A. Luo, J.J. Jonas, Scr. Mater. 55 (2006) 1055–1058.
[18] M. Humbert, N. Gey, J. Muller, C. Esling, J. Appl. Cryst. 29 (1996) 662–666.
[19] X. Li, W. Qi, Mater. Sci. Eng. A 560 (2013) 321–331.
[20] M.Y. Wang, R.L. Xin, B.S. Wang, Q. Liu, Mater. Sci. Eng. A 528 (2011) 2941–2951.
[21] Y.B. Chun, C.H.J. Davies, Mater. Sci. Eng. A 556 (2012) 253–259.